J. metamorphic Geol., 2002, **20,** 801–812

Numerical simulations of spiral-shaped inclusion trails: can 3D geometry distinguish between end-member models of spiral formation?

A. STALLARD*, H. IKEI† AND T. MASUDA
Institute of Geosciences, Shizuoka University, Shizuoka, Japan (a.stallard@geol.canterbury.ac.nz)

ABSTRACT Numerical 3D simulations of the development of spiral inclusion trails in porphyroblasts were conducted in order to test the proposals that (a) 3D spiral geometry differs between the rotation and nonrotation end-member models of spiral formation proposed in the literature, and (b) 3D spiral geometry can be used as a criterion to distinguish between the two end-member models in rocks. Four principal differences are identified between the two sets of simulations: smoothness of spiral curvature; spacing of foliation planes; alignment of individual foliation planes either side of the sphere representing the porphyroblast; and spiral asymmetry with respect to matrix shear sense. Of these differences, only spiral asymmetry and possibly the alignment of individual foliation planes are diagnostic criteria for distinguishing between the end-member models. In the absence of a readily applied test to distinguish the end-member models, interpretation of spiral inclusion trails is problematic. It is necessary to determine complementary evidence to distinguish porphyroblast rotation or nonrotation during spiral formation.

Key words: numerical simulation; porphyroblast; spiral inclusion trails.

INTRODUCTION

Spiral inclusion trails within garnet porphyroblasts are a feature of schistose rocks within many of the worlds orogenic belts (e.g. Rosenfeld, 1970; Schoneveld, 1978; Johnson, 1993a). The formation of spiral trails was originally explained by the progressive capture of the matrix foliation within a growing porphyroblast that rotated during foliation-parallel shear (e.g. Spry, 1963; Passchier *et al*., 1992). An alternative to this model involves rotation of the matrix foliation around an irrotational porphyroblast, which was first proposed by Ramsay (1962) and Powell & Treagus (1970). More recently, Bell & Johnson (1989) argued that spirals form by irrotational garnet growth over multiple overprinting near-orthogonal foliations. For the sake of brevity, these two end-member models will be referred to as the rotation (e.g. Passchier *et al*., 1992) and nonrotation (e.g. Bell & Johnson, 1989) models.

The relative merits of the different models of spiral development have been widely debated (e.g. Bell *et al*., 1992b; Passchier *et al*., 1992; Visser & Mancktelow, 1992; Forde & Bell, 1993; Johnson, 1993b; Williams & Jiang, 1999), but conclusive testing of each model has been made difficult by the lack of diagnostic criteria for distinguishing between the competing models in rocks. This is largely because the central element of both models is the *relative* rotation of porphyroblast and matrix, and as such, most, if not all inclusion trail patterns can be produced by either model (e.g. Powell & Treagus, 1970; Johnson, 1993b). The significance of this debate extends beyond the obvious question of whether or not the porphyroblasts rotated relative to a fixed reference frame, as the mode of spiral formation has important implications for our interpretation of shear sense (e.g. Bell & Johnson, 1992), fold mechanisms (e.g. Visser & Mancktelow, 1992; Stallard & Hickey, 2001b), crenulation development and microstructural history of deformation (e.g. Stallard, 1998).

In an attempt to demonstrate that the end-member models result in different geometries, Williams & Jiang (1999) compared the 3D geometry of a theoretical nonrotation spiral with a rotation spiral produced by the mechanical model of Schoneveld (1977, 1979). The authors concluded that 3D spiral geometry is model specific, although they did not identify the geometric features that distinguish the two models.

The aim of this study is to use numerical simulations to test for diagnostic differences in the 3D geometry of spiral inclusion trails produced by the competing models. The degree of similarity between the resulting simulated trails is then assessed to test if the 3D geometry might provide criteria for determining the origin of spiral inclusion trails in rocks.

3D SIMULATIONS

Hydrodynamic model

The numerical simulations presented in this study are based on the 3D hydrodynamic model of Masuda & Ando (1988) and Masuda & Mochizuki (1989). The porphyroblast and matrix are modelled numerically as a rigid sphere embedded in a homogeneous Newtonian

* Now at: Department of Geological Sciences, University of Canterbury, Christchurch, New Zealand.
† Now at: Kiso-Jiban Consultants Co. Ltd, Tokyo 102–8220, Japan.

viscous fluid. Deformation of the matrix is dextral simple shear far from the sphere, and the sphere rotates at a rate equal to half the far field simple shear strain rate. The velocity vector is continuous and equal to zero at the interface between the sphere and matrix, and there is no slip at the interface. The radius of the sphere increases at a constant rate of volume, and growth is assumed to involve volume-for-volume replacement of the fluid matrix. Marker particles are set in the matrix to represent the foliation, and these move passively as the matrix deforms, while those included in the growing sphere rotate as the sphere rotates.

Description of rotation and nonrotation simulations

For the purpose of numerical simulation, the rotation and nonrotation models are each defined in their most simple form, while retaining the essential elements that distinguish the respective models. Both sets of simulations were run until the far field shear strain reached gamma = 8. Porphyroblast rotation in the numerical simulations is described relative to the simulation boundaries. In the rotation simulation, a single generation of matrix foliation is deformed by foliation-parallel simple shear, which results in rotation of the sphere (Fig. 1a; see also Masuda & Mochizuki, 1989; Bjornerud & Zhang, 1994; Gray & Busa, 1994). The nonrotation simulation involves matrix deformation, without sphere rotation, during the development of four overprinting orthogonal foliations (Fig. 1b).

This study is the first to simulate numerically the nonrotation model. While the physics of matrix flow around the sphere is the same in both models, the nonrotation simulation involved three additional complications. First, the nonrotation simulation involves four overprinting foliations. Each change in foliation was modelled by rotating the simulation shear plane 90°, while ensuring that shear sense was kept constant (i.e. consistently clock-wise or anticlockwise during the course of the simulation). The timing of each new foliation was decided at the stage where the currently deforming matrix foliation, adjacent to the sphere, had developed approximately 90° rotation relative to the sphere (Fig. 1b).

Second, the Bell (1985) nonrotation model of porphyroblast growth involves partitioning of matrix deformation into zones of coaxial shortening close to the porphyroblast, and zones of noncoaxial strain that anastomose around the porphyroblast. Such a pattern of strain partitioning is too complex to model numerically, so the matrix deformation was modelled under conditions of simple shear. We consider this to be an adequate approximation for the following reason. In the nonrotation model, inclusion trail curvature, and ultimately spiral-shaped inclusion trails, originate from crenulation of the matrix foliation in zones of *noncoaxial* strain (cleavage seams of a developing crenulation cleavage) adjacent to the growing porphyroblast. The curved foliation is later included within the porphyroblast as it grows toward, and eventually over the adjacent cleavage seam. Thus, although Bell (1985) described the porphyroblast as occupying a zone of coaxial strain, it is more appropriate to deform the matrix by noncoaxial shear. The simulation does not include an area of coaxial strain adjacent to the sphere, but the velocity vector in those areas is extremely low (light grey areas to the left and right of the sphere in Fig. 2b), indicating minimal particle movement.

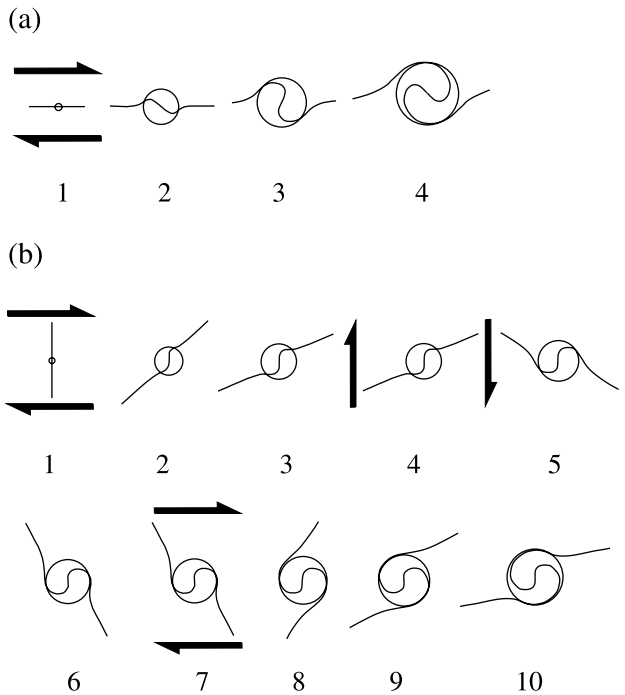

Fig. 1. Schematic description of the rotation and nonrotation simulations used in this study. (a) Rotation simulation. A single generation of matrix foliation is deformed by foliation-parallel simple shear. Inclusion trails are rotated within the rotating sphere. (b) Non-rotation simulation. The irrotational sphere grows during the development of four overprinting orthogonal foliations. The pre-existing foliation is oriented at 90° to the shear plane. New foliations are initiated at stages 1, 4 and 7 as shown in the figure. Inclusion trails remain irrotational within the sphere. This figure is schematic only, and the numbered stages of each simulation represent the sequential development of the simulation rather than equal intervals of time or spiral development.

Third, the nonrotation model describes nonrotation of porphyroblasts within local zones of coaxial strain. The numerical simulation used in this study cannot partition the deformation in this way, and thus the pattern of matrix velocity in the nonrotation simulation should theoretically result in sphere rotation. In order to solve this inconsistency, we imposed a condition of nonrotation upon the sphere (parameter k of Bjornerud & Zhang, 1994), and removed the spin-related part of the velocity field (the total velocity field is calculated from two components: the matrix velocity vector and the component of shear due to effect of rotation of sphere on surrounding matrix). This does

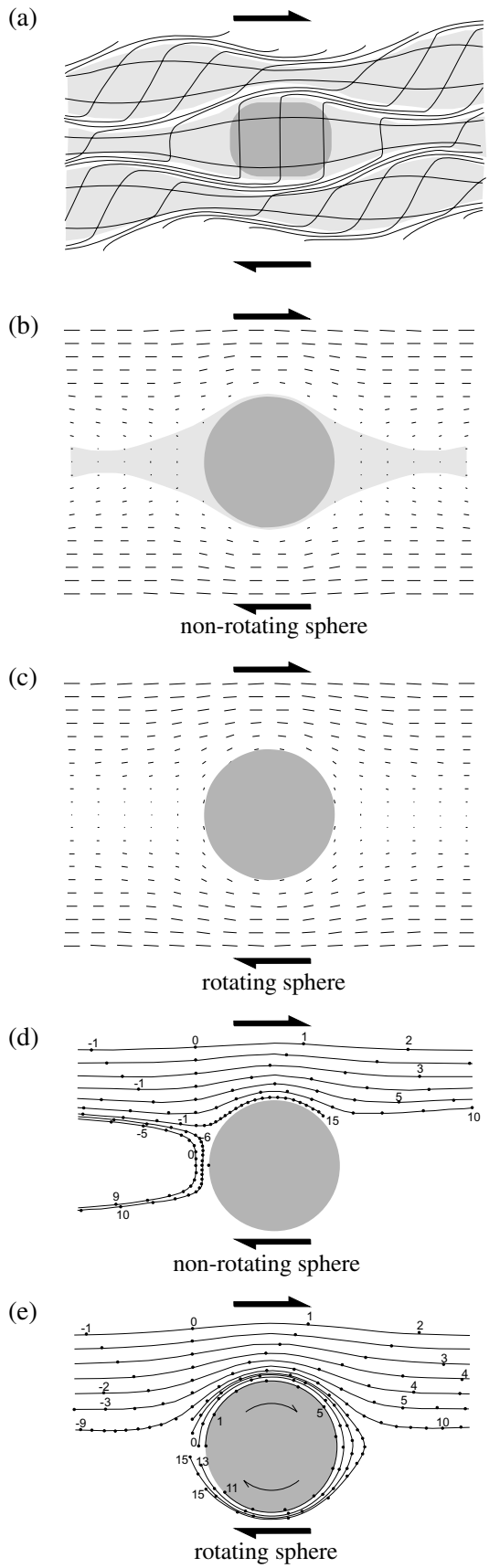

not affect the validity of the physics of matrix fluid flow (and particle movement) around the nonrotating sphere.

Figure 2 shows the velocity vector and particle path plots for both the rotation and nonrotation simulations presented in this study, as well as a comparison with Bell's (1985) nonrotation model. The particle path in the rotation simulation (Fig. 2e) is similar to those previous published (e.g. fig. 1 of Pennacchioni *et al*., 2000), while the nonrotation particle path (Fig. 2b) resembles Bell's (1985) deformation partitioning model (Fig. 2a).

As noted by Johnson (1999), both the rotational and nonrotational models can be modified in various ways to account for specific geometries that are not predicted by the models in their simplest forms. This may involve varying the amount of flattening in the matrix (e.g. Williams & Jiang, 1999), the ratio of pure to simple shear (Mandal *et al*., 2001), the timing and rate of porphyroblast growth relative to deformation (Bjornerud & Zhang, 1994), the rate of porphyroblast rotation (e.g. Biermeier *et al*., 2001), or the geometry of the predeformation foliation relative to the shear plane (e.g. Masuda & Mochizuki, 1989). In this study, the two models are compared in their most basic forms in order to test for first-order or diagnostic differences in the resulting 3D inclusion trail geometries. Additional simulations were conducted to assess the variation in 3D spiral geometry resulting from modification of the basic models, and these are discussed later.

Limitations of hydrodynamic model

The numerical modelling employed in this study involves limitations and assumptions resulting from the necessary numerical simplification of a complex

Fig. 2. Velocity vector and particle path plots of simulations used in this study, and comparison of nonrotation simulation with the nonrotation model as described by Bell (1985). (a) Strain partitioning model of Bell (1985). The porphyroblast (dark grey) lies within a field of noncoaxial strain (light grey) and thus does not rotate with respect to shear plane. Strain is partitioned into zones of shear (white) that are represented by cleavage seams in real rocks. In this figure, adjacent microlithons do not house porphyroblasts, and thus strain within these areas is noncoaxial. (b) Velocity vector field of the nonrotation simulation used in this study. The lengths of the bars indicate the relative magnitude of the velocity, and the orientation indicates direction. The spherical porphyroblast (dark grey) is surrounded by a field of low flow velocity (light grey), although deformation is not coaxial in this zone (cf. Fig. 2a). The areas of higher matrix velocity (white areas) undergo noncoaxial shear, which corresponds to the white areas in (a). The simulation represents the central microlithon, porphyroblast and adjacent zones of shear shown in (a). (c) Velocity vector field for the rotation simulation. (d,e) Particle path fields for the nonrotation and rotation simulations, respectively. The numbers represent the magnitude of far field shear strain from the beginning of deformation (0). Figures (c) and (e) are modified from Masuda & Ando (1988).

natural system. The heterogeneous rock matrix is modelled as a homogeneous fluid, and the porphyroblast as a perfect sphere. Important strain accommodation such as crenulation development, recrystallization, and grain-scale deformation processes are not simulated. In the nonrotation simulation, we impose a condition of nonrotation upon the sphere, although under the physical conditions of the simulation the sphere should rotate. These kinds of limitations are common to previous studies of spiral development (Masuda & Mochizuki, 1989; Bjornerud & Zhang, 1994; Gray & Busa, 1994), but do not preclude the geologic relevance and value of such an investigation. Thus, the modelling provides a useful and instructive approximation of the end-member models, and provides an advance in the interpretation of these controversial microstructures.

Simulation results

Description of simulation results

The simulation results are presented in Figs 3 & 4. Figure 3 shows cut-away geometries of the 3D spirals, and equivalent matrix foliation, for both the rotation and nonrotation simulations. Figure 4 shows a series of 2D sections through the simulated inclusion trails and equivalent matrix foliation.

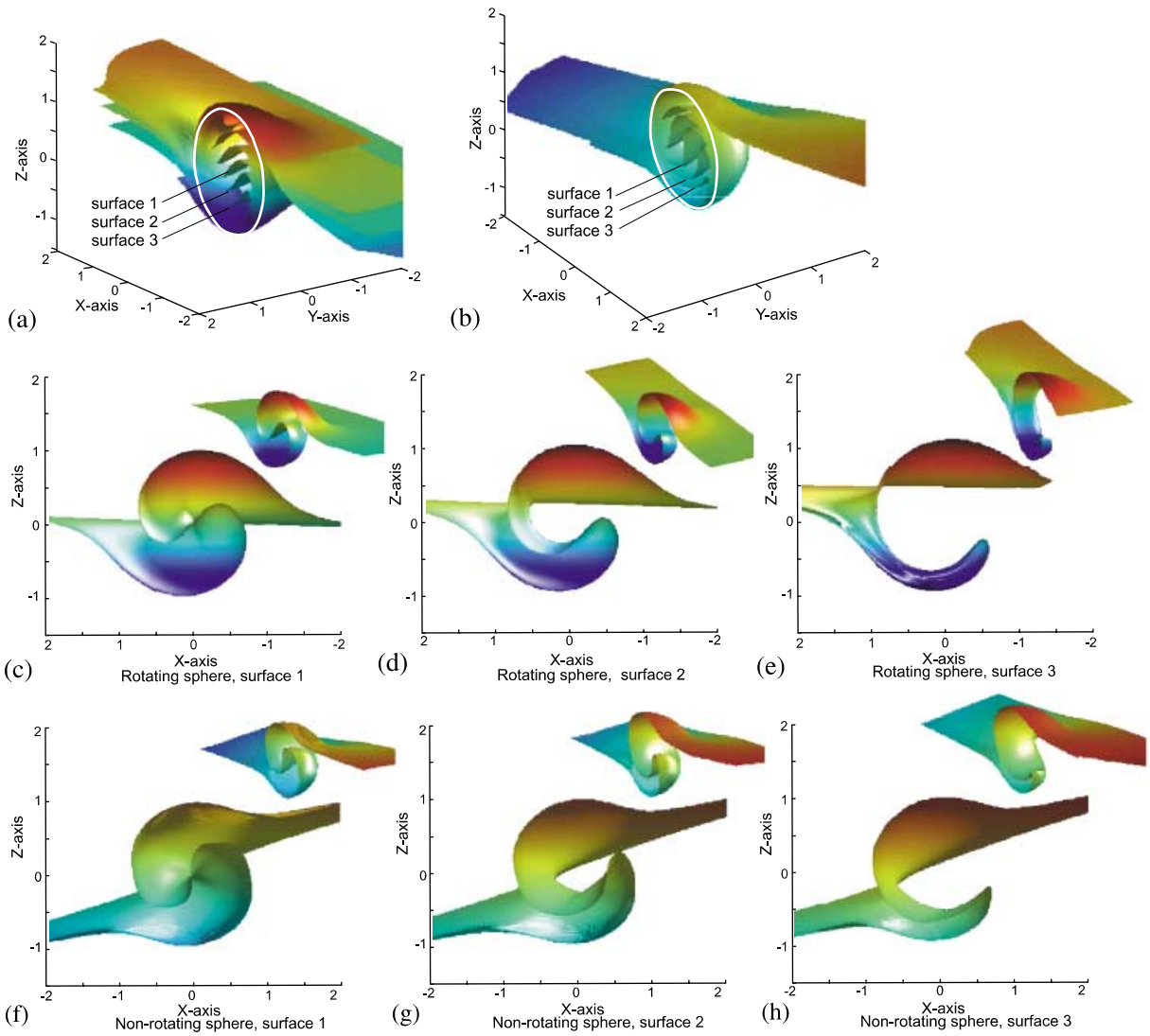

Fig. 3. Comparison of the 3D geometry of the rotation and nonrotation simulations. (a) and (b) show the rotation and nonrotation simulations, respectively, with the spheres outlined in white. The three surfaces labelled on each simulation are shown separately in Figs (c)–(h) to illustrate the varied geometry of surfaces located at increasing distances from the porphyroblast centre. The rotation and nonrotation simulations are viewed from opposite directions in order to enable direct comparison of the two sets of geometries. The fine scale wrinkles visible in the lower parts of (f) (g) and (h) are due to the limits of resolution of the simulation, and are not real features of the spiral geometry.

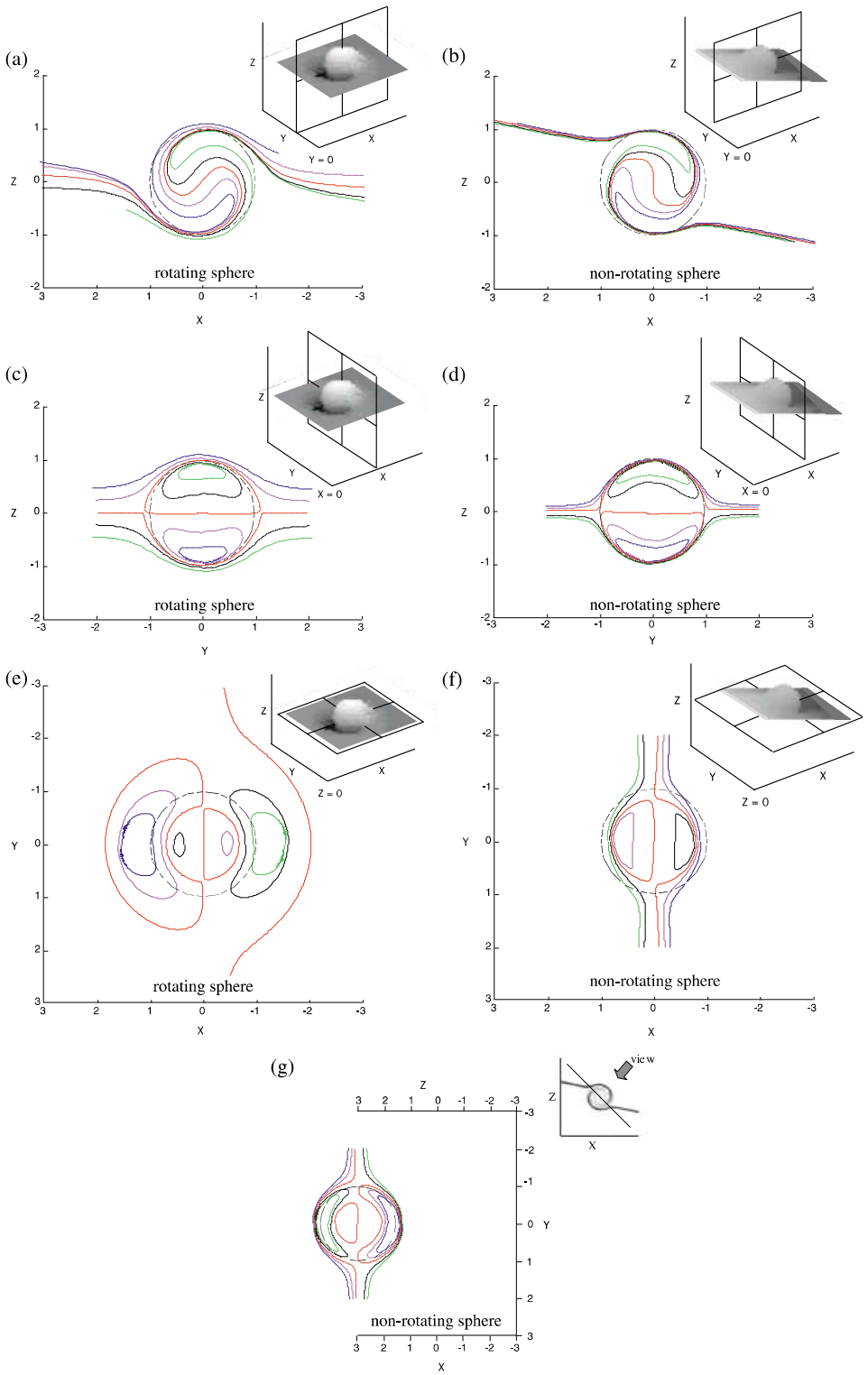

Fig. 4. Comparison of 2D sections through the rotation and nonrotation simulations. (a, b) sections parallel to the XZ plane. (c, d) sections parallel to the YZ plane. (e, f) Sections parallel to the XY plane. (g) Oblique section through the nonrotation simulation. Although (e) and (f) are both sectioned in the XY plane, it is more appropriate to compare (e) with a section from the nonrotation simulation that also intersects the matrix foliation planes adjacent to the sphere. This results in the closed loops that straddle the sphere margin. Equivalent colours represent equivalent surfaces in different sections of each simulation. Subplots show orientation of each 2D section with respect to the simulation boundaries. In all figures, the sphere is represented by a dashed black circle.

In the rotation simulation, the matrix foliation wraps around the growing porphyroblast and results in a complex noncylindrical geometry. Once captured within the sphere, the foliation is progressively rotated away from the equivalent foliation in the matrix, forming a smoothly curving spiral geometry. The central inclusion surface forms a doubly curving noncylindrical geometry, which resembles a symmetrical pair of sheath folds that once formed, are progressively enlarged, rotated and stretched about the axis of relative rotation between the sphere and matrix (Fig. 3c). Planes 2 and 3 are positioned off-centre with respect to the growing sphere and can be visualised as single sheath folds that are progressively elongated and rotated about the axis of relative rotation as the sphere grows (Fig. 3d,e).

In the nonrotation simulation, the spiral geometry results from rotation of the matrix around the irrotational porphyroblast. As with the rotation simulation, the matrix wraps around the sphere, and it is this shape that is included within the growing sphere to define the 3D geometry of the spiral (Fig. 3b,f). From the centre to the rim of the sphere, the central inclusion plane contains intervals of relatively gentle curvature separated by intervals of relatively tight curvature, and is not as smoothly curving as the rotation simulation.

In both sets of simulations, surfaces originally positioned at progressively greater distances from the sphere centre have sheath fold geometries that are narrower and less elongate when viewed in the XZ plane (Fig. 3e,h). Cross-sections through these sheath folds geometries reveal closed-loop inclusion trail patterns (Fig. 4c,d).

The simulation results presented in this study are broadly consistent with the model spiral geometries previously published by Powell & Treagus (1967, 1970), Masuda & Mochizuki (1989), Bjornerud & Zhang (1994), Gray & Busa (1994), and Schoneveld (1977), and with the sections through garnet published by Johnson (1993a). The simulations are however, different to Williams & Jiang's (1999) theoretical interpretation of the 3D geometry of spirals formed according the nonrotation model. These differences result from interpretations by Williams & Jiang regarding the nature of matrix deformation around a growing porphyroblast (see Johnson, 1999 for more on this subject).

Comparison of results of rotation and nonrotation simulation

At first glance, the 3D geometry of the rotation and nonrotation simulations is very similar (Figs 3 & 4). The apparent differences between the two simulations in the 2D XY sections (Fig. 4e,f) occurs because at the time the nonrotation simulation finished, the foliation planes within the matrix did not cross the $Z = 0$ plane (*cf.* rotation simulation). Given further running-time of the simulation, the nonrotation foliation planes would soon rotate into a position comparable to those in the rotation simulation. Although both figures (Fig. 4e,f) are oriented in the same way with respect to the simulation boundaries, they do not offer a valid comparison of equivalent sections through the spirals with respect to the position of the spiral and matrix foliations. To illustrate this point, we re-sectioned the nonrotation simulation in an orientation that intersects the matrix foliation planes. The resulting 2D geometry (Fig. 4g) is more comparable to that of the equivalent section cut through the rotation simulation (Fig. 4e).

Comparison of the two sets of simulations reveals the following four differences between the 3D geometry of the end-member models:

(1) Smoothness of spiral curvature. The rotation simulation displays a relatively smoothly curving central inclusion trail surface, whereas the central inclusion plane of the nonrotation simulation is marked by intervals of gentle curvature separated by narrow zones of relatively tight curvature (compare Fig. 3c with Fig. 3f). These differences reflect the number of matrix foliations developed during sphere growth in each simulation. The rotation model describes sphere growth within a single foliation. Once the matrix foliation has wrapped around the nucleated porphyroblast, the relative orientations of the matrix and inclusion trails reaches a steady-state and a relatively smooth spiral results. The only variation in spiral curvature occurs in the very centre of the sphere, where a section of planar inclusion trails represent the earliest portion of included matrix foliation (e.g. Fig. 4a). In contrast, the nonrotation simulation involves sphere growth that spans the development of four distinct matrix foliations (Fig. 1). At the initiation of each new foliation, the existing matrix foliation is oriented at approximately 90° to the new direction of shear, and is thus quickly rotated toward the shear plane. The variably curving spiral represents cycles of rapid rotation of the foliation about the sphere coincident with the development of a new foliation, and periods of slower rotation as the foliation matures and is reoriented closer to the shear plane.

(2) Spacing of foliation planes. Neighbouring foliation planes in the nonrotation simulation are more closely spaced and more tightly wrapped around the sphere than equivalent foliation planes in the rotation simulation (compare Fig. 4c with 4d, and Fig. 4e with 4g). This occurs because the angular relationship between the foliation planes and shear plane is different in the two simulations. Reduction in the spacing between foliation planes occurs while the matrix foliation is oriented at a high angle to the shear plane, and also as the foliation is progressively wrapped around the sphere. During the course of the nonrotation simulation, the angular relationship between the shear plane and matrix foliation varies continuously (Fig. 1b), and the foliation planes become closely spaced in all orientations within the

matrix as well as adjacent to the sphere. In contrast, the rotation simulation involves sphere growth within a single foliation that is always oriented at a low angle with respect to the shear plane. The spacing between planes is reduced only in those areas close to the sphere and shortening occurs dominantly parallel to the Z axis. The XY plane contains the greatest contrast in the spacing of foliation planes between the two simulations (e.g. compare Fig. 4c,e with Fig. 4d,g, respectively).

(3) Alignment of foliation planes either side of the sphere. A further difference between the two simulations is the alignment of individual foliation planes on opposite sides of the sphere. The rotation simulation creates deformation of the matrix within a small volume surrounding the sphere, and those parts of individual foliation planes at greater distances from the sphere remain less deformed. A single dashed line can be drawn to join aligned sections of an individual foliation plane either side of the sphere (Fig. 5a). In contrast, the nonrotation simulation involves deformation of all parts of the matrix foliation, including those areas further from the sphere, and consequently individual foliation planes are not aligned either side of the sphere (Fig. 5b).

(4) Spiral asymmetry with respect to matrix shear sense. The rotation and nonrotation simulations display contrasting relationships between spiral asymmetry and matrix shear sense (compare Fig. 4a with 4b). This relationship has been described previously (e.g. Bell & Johnson, 1989) and is established as a diagnostic criterion for distinguishing between the two models (e.g. Johnson, 1993b).

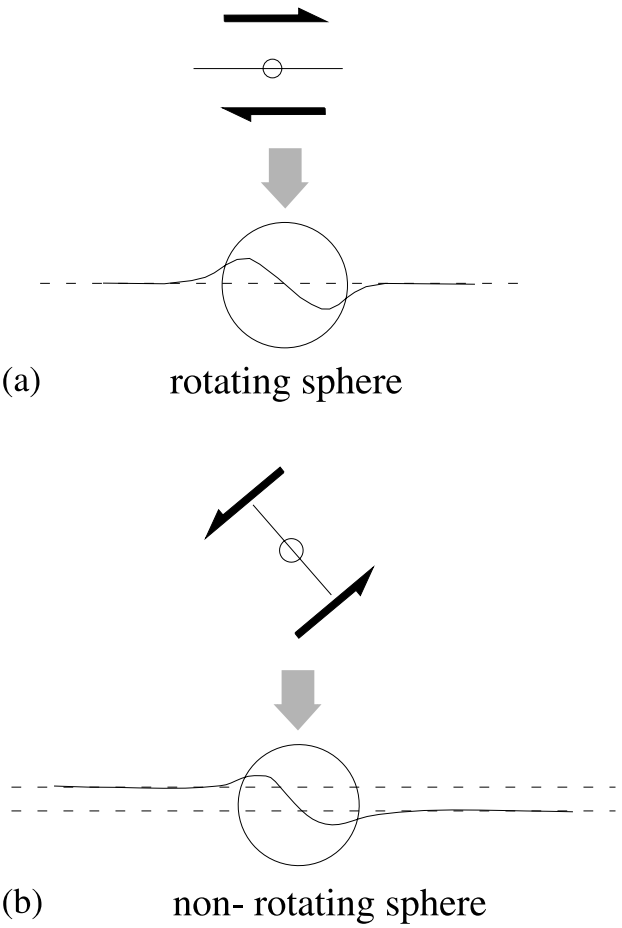

Fig. 5. Comparison of the deformation of individual foliation planes produced by the rotation and nonrotation simulations. (a) During the rotation simulation, those parts of a foliation plane distant from the sphere are relatively undeformed, and remain aligned either side of the sphere. (b) During the nonrotation simulation, all parts of the foliation plane are deformed, and those parts of an individual foliation plane either side of the sphere become unaligned.

DISCUSSION

Are the differences between the simulations diagnostic of the end-member models?

Having described the principal differences between the two simulations, we now consider if these differences are diagnostic and therefore provide a means of distinguishing between the end-member models in rocks. Each of the four main differences between the two simulations described in the previous section is considered below.

(1) Smoothness of spiral curvature. Given the end-member models in their most simple forms, the central inclusion surface produced by the rotation model is likely to be more smoothly curving than the equivalent surface resulting from the nonrotation model. This criterion applies to the central inclusion surface when viewed in the XZ section (e.g. Fig. 3c,f). However, in rocks the spiral curvature may be influenced by factors such as discontinuous porphyroblast growth, porphyroblast growth that is not radially continuous (Passchier *et al*., 1992), and the control of crystal face geometry (e.g. fig. 4 of Johnson, 1993b). Careful mapping of inclusion trail patterns has shown that spirals which initially appear smoothly curving and continuous from core to rim are commonly characterised by varying inclusion trail curvature, and even truncations of the inclusion trails (e.g. Bell & Johnson, 1989; Bell *et al*., 1992a). This criterion may be used to support an interpretation, but is probably not diagnostic of either end-member model.

(2) Spacing of foliation planes. Foliation planes are more closely spaced in the nonrotation simulation than the rotation simulation, but this criterion is likely to be both difficult to apply, and less pronounced in rocks. There are three main reasons for this. First, in the nonrotation simulation, the length of rotated (deformed) foliation planes is restricted to the spacing of cleavage domains of the newly formed foliation.

This restricts the rotation of foliation planes to within the confines of individual microlithons. The process of crenulation is not included in the numerical simulations, and thus the close spacing of foliation planes developed during the simulations is likely to be less pronounced in rocks. Second, a component of flattening normal to the XY plane in the rotation simulation would act to reduce the spacing between adjacent foliation planes and produce a geometry more similar to that of the nonrotation simulation. Third, the successful application of this criterion to rocks is dependant upon knowledge of the spacing between foliation planes prior to spiral formation compared with the spacing after spiral formation, and this may be difficult to determine. The spacing of foliation planes is a criterion not easily applied to rocks and is probably not diagnostic of either end-member model.

(3) Alignment of foliation planes either side of the sphere. This criterion can be applied in rocks containing a planar matrix foliation and inclusion trails continuous with the external foliation (Fig. 5). The relationships shown in Fig. 5 will not hold true if the angle between the matrix foliation and shear plane (in the rotation simulation) changed during the course of the simulation, or had an initial nonzero value. Assuming a constant angular relationship between matrix foliation and shear plane, it is possible that this criterion is diagnostic.

(4) Spiral asymmetry with respect to matrix shear sense. The relative shear sense of spiral and matrix is a distinguishing criterion between the two models, provided that inclusion trails are continuous with the matrix foliation and that matrix shear is demonstrated to be contemporaneous with spiral formation. A synthetic sense of shear between inclusion trail curvature and matrix indicates spiral formation according to the nonrotation model, whereas antithetic shear is consistent with the rotation model (see Fig. 1 of Hickey & Bell, 1999). However, establishing the matrix shear sense synchronous with spiral growth is commonly difficult to determine (see Johnson, 1993b; p654). Previous studies have reported examples of inclusion trail asymmetry that are apparently consistent with the rotation model (e.g. Busa & Gray, 1992) and that are apparently consistent with the nonrotation model (Treagus, 1987; Bell & Johnson, 1992).

The simulations conducted in this study compare the rotation and nonrotation models in their most basic forms, but if 3D geometry is to be used as a criterion for distinguishing the two models in rocks, the full range of spiral geometries that each model might generate must first be considered. To investigate this further, we conducted simulations to assess the effect on spiral geometry of varying certain simulation conditions (Fig. 6). These simulations reveal that growth rate does not affect spiral geometry (Fig. 6a), but an increase in the component of pure shear (in the rotation simulation) results in decreased rotation between sphere and matrix, and reduced spacing between foliation planes (Fig. 6c). An increase in the initial angle between the matrix foliation and shear plane (theta) results in reversals in the asymmetry of the inclusion trails (Fig. 6b). The reversals develop due to changes in the rate of rotation of the matrix foliation and sphere at the critical theta values of 135° and 45° (see Masuda & Mochizuki, 1989). Once the matrix foliation has been reoriented close to the shear plane, inclusion trails develop a more regular spiral geometry. The geometries shown in Fig. 6(b,c) suggest that the two models can produce a wide range of similar geometries and highlight the problems in finding diagnostic criteria to distinguish the two end-member models in rocks. For example, a component of pure shear reduces the spacing between foliation planes in the rotation simulation, and thus creates uncertainty in the use of spacing between foliation planes as a criterion that potentially distinguishes the rotation and nonrotation simulations (see above). Increased values of theta affect the smoothness of spiral curvature produced by the rotation simulation, and results in reversals of inclusion trail asymmetry that might mistakenly be interpreted as representing discreet deformation events (cf. fig. 5 of Bell *et al.*, 1998).

Why do contrasting models produce apparently similar 3D simulation results?

While we have identified four principal differences between the two simulations, the overall 3D geometry of the spirals is surprisingly similar (Fig. 3). This occurs despite differences in the initial conditions of the respective simulations. These differences include: the number of matrix foliations developed during sphere growth (Fig. 1), the respective velocity vectors and particle paths in the rock mass surrounding the sphere (Fig. 2), and the distribution of strain within the matrix. The 3D geometries are more similar than what might be expected given the above differences in the initial conditions of the two simulations, and the reasons for this are discussed, in terms of the principal differences between the two simulations, in the following sections.

Velocity vector and particle path (Fig. 2)

Differences in the velocity vector and particle path plots for the rotation and nonrotation simulations primarily reflect the contribution of the spin-related part of the velocity field in each model. The rotation model describes simple shear and sphere rotation, and results in an eye-shaped flow perturbation about the sphere (Fig. 2e). A separatrix surface (see Passchier *et al.*, 1993) marks the boundary between closed elliptical displacement paths close to the sphere, and open displacement paths further away. In contrast, the spin-related component of the nonrotation velocity

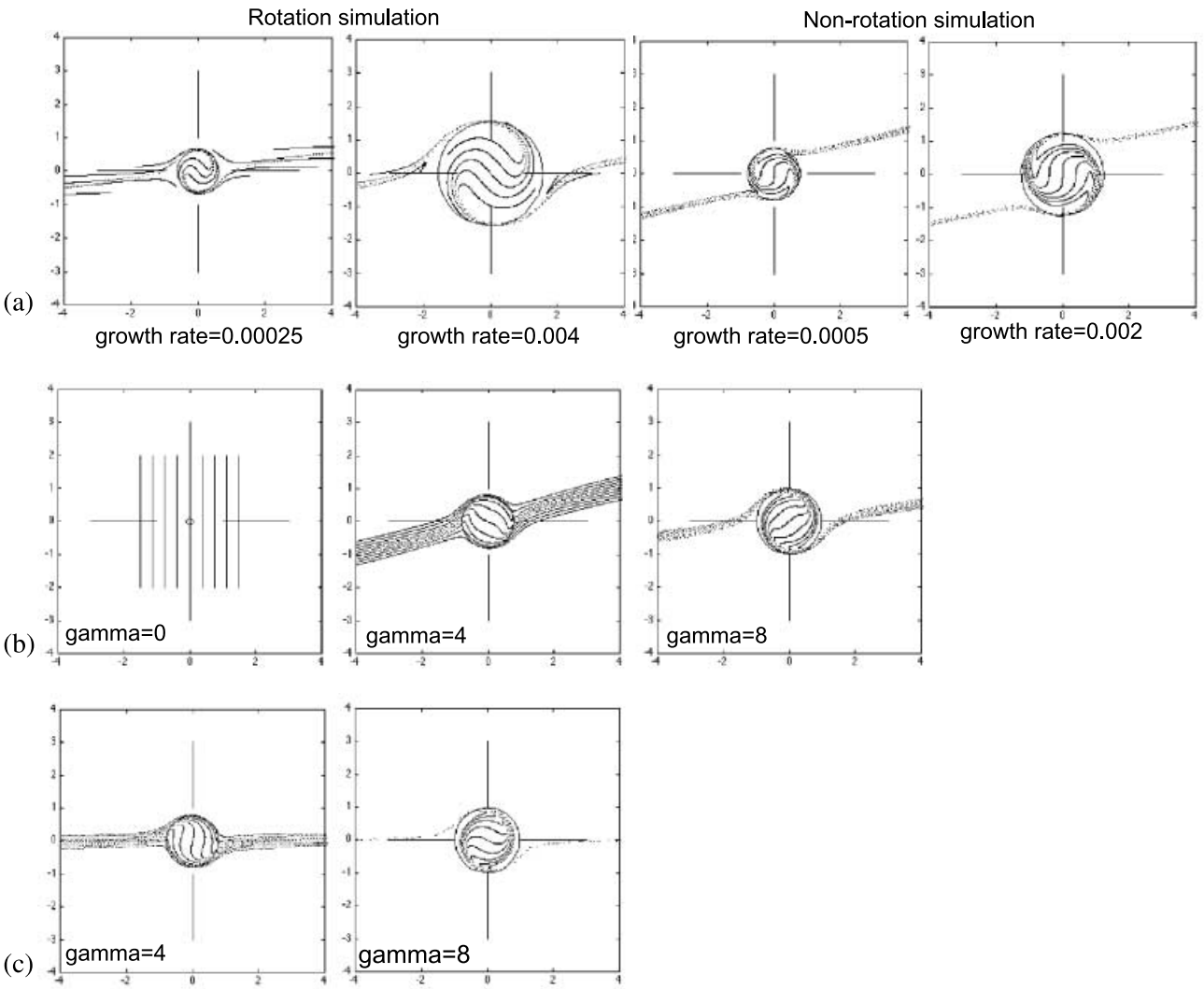

Fig. 6. Summary of varying spiral geometry resulting from changes to sphere growth rate, matrix strain type, and initial angle between matrix foliation and shear plane. (a) Completed simulations (gamma = 8) at different rates of sphere growth. The growth rate of the simulations shown in Figs 3 and 4 is 0.001 per time step of the simulation. (b) Rotation simulation with initial angle between matrix foliation and shear plane (theta) of 90°. The theta value of the rotation simulations shown in Figs 3 and 4 is 0°. (c) Rotation simulation with ratio of simple shear to pure shear = 2. Compare this with the simulations shown in Figs 3 and 4, which involved simple shear matrix deformation with no component of pure shear. All sections shown in this figure are XZ sections.

field is equal to zero, and a bow-tie shaped flow pattern results (Fig. 2d). Separatrix surfaces either side of the sphere (as viewed in Fig. 2d) mark the boundary between areas of open displacement paths above and below the sphere, and flow paths either side of the sphere that first move toward, then away from the sphere. The areas of principal difference in the respective particle paths occur either side of the sphere (as viewed in Fig. 2d,e), in zones that are usually occupied by strain shadows in rocks.

Despite the differences, the contrasting particle paths produce only minimal differences in the resulting simulation geometries, for which we suggest two reasons. First, the areas of contrasting particle paths between the two simulations (areas either side of the spheres in Fig. 2d,e) are areas of low flow velocity, whereas areas that contain similar particle paths (areas above and below spheres) have large flow velocity. This means that areas of contrasting matrix deformation develop slowly compared to areas with similar deformation patterns, and this acts to minimise differences in the spiral geometry between the two models. Second, with the development of each new foliation in the nonrotation model, the velocity vector and particle path fields are rotated by 90° with respect to the sphere (see Fig. 1b, steps 4 and 8). Areas that were within the low-velocity zone adjacent to the sphere during development of the first foliation are located within the high-velocity zone during development of the second foliation. In this way, the relatively

slowly developing areas of contrasting geometry adjacent to the sphere are quickly overprinted during the succeeding foliation to produce a geometry that is similar in both models.

Distribution of strain

Whereas the rotation model involves highly noncoaxial simple shear deformation, Bell (1985) explained porphyroblast nonrotation as a consequence of strain partitioning into zones of noncoaxial strain and zones of coaxial shortening. Despite these differences in strain distribution, both models contain common elements of spiral development. In both models, foliation curvature, which is the essence of spiral formation, occurs within zones of noncoaxial shear in the matrix adjacent to the growing sphere. As the porphyroblast grows over the adjacent zone of noncoaxial shear, the curved foliation planes are included within the porphyroblast to form a spiral geometry.

Matrix foliations

The rotation model describes porphyroblast growth within a single matrix foliation of consistent orientation, whereas the nonrotation model involves repeated cycles of crenulation and foliation development to account for spiral formation (e.g. Bell & Johnson, 1989). Although we don't consider the number of foliations to result in diagnostic differences in the 3D spiral geometry, evidence of multiple foliations preserved within the porphyroblast does support the nonrotation model (e.g. figs 4 & 5 of Stallard & Hickey, 2001a).

Testing the rotation and nonrotation models

Previous studies have proposed a number of criteria for discriminating between the rotation and nonrotation models in rocks. These include 3D inclusion trail geometry (e.g. Williams & Jiang, 1999), inclusion trail orientations over a large area (e.g. Johnson, 1990), specific inclusion trail microstructures (fig. 10 of Johnson, 1993a; p. 182 of Passchier & Trouw, 1996), spiral axis orientations over a large area (e.g. Bell *et al.*, 1998), and matrix shear sense during porphyroblast growth (Johnson, 1993b). The application of these criteria to rocks has proven controversial. For example, Johnson (1993b) concluded that most, if not all, inclusion trail geometries in spiral porphyroblasts can be explained by either model, and that 3D geometry and specific microstructures are not diagnostic of the competing models (cf. Williams & Jiang, 1999). Interpretation of inclusion trail orientation data is also a debated topic. The consistent orientation of inclusion trails over a large area has been interpreted to support the nonrotation model (e.g. Johnson, 1990), but Jiang (2001) has cautioned that such patterns are a natural consequence of vorticity during folding, and do not necessarily indicate that porphyroblasts remained irrotational during deformation (see also Kraus & Williams, 2001). The interpretation of individual microstructures preserved within porphyroblasts has also been a subject of debate (e.g. Passchier *et al.*, 1992; Gray & Busa, 1994; Johnson & Bell, 1996). Bjornerud & Zhang (1994) suggested that the geometry of mica 'haloes' adjacent to spiral porphyroblasts reflect the degree of porphyroblast rotation during spiral formation. This proposal can be further evaluated once the interaction of multiple flow patterns can be successfully modelled (e.g. Samanta *et al.*, 2002).

A different approach to the problem is to consider the deformation environment in which the porphyroblasts grew (e.g. Stallard & Hickey, 2001a), as each model predicts a different deformation environment for spiral formation. Descriptions of the rotation model usually describe spiral development within a shear zone (e.g. Williams & Jiang, 1999), whereas the nonrotation model describes multiple episodes of crenulation, folding and foliation formation.

It is also possible that a combination of processes occurs in nature, and that porphyroblasts grow in a folding environment in which the spiral geometry is largely the result of overprinting foliations, although accompanied by some net rotation of the porphyroblast relative to fold axial planes (e.g. Stallard & Hickey, 2001b). In this scenario, the spiral geometry reflects accumulated crenulation events, in accordance with the nonrotation model, although it remains difficult to quantify the net porphyroblast rotation with respect to fold axial planes. In such a situation, the geometric relationship between inclusion trails and matrix folds provides a means of estimating the amount of porphyroblast rotation (e.g. Williams & Jiang, 1999; Stallard & Hickey, 2001b; Jiang, 2001). This line of investigation is important, as spiral garnets are commonly found in multiply folded terranes in rocks that preserve multiple foliations and crenulation cleavages (e.g. Bell *et al.*, 1998; Mares, 1998; Stallard & Hickey, 2001a; Williams *et al.*, 2001). Such an approach may lead to more realistic models of spiral development that incorporate elements of both the rotation and nonrotation models and link spiral formation to fold mechanisms and the competence of rocks at the time of folding.

In summary, any interpretation concerning the mode of spiral formation is best supported by a suite of complementary evidence that may include 3D spiral geometry, matrix shear sense, microstructures preserved within the porphyroblast (e.g. crenulation cleavages), spiral axis orientation patterns, and the alignment of individual foliation planes within the matrix. Ideally, the minimum data required for such an exercise includes detailed 3D analysis of spiral geometry from multiple samples within the area of study, and detailed microstructural and kinematic information from the rock matrix.

CONCLUSIONS

Numerical simulations reveal four principal differences in the 3D geometry of spiral inclusion trails produced by the rotation and nonrotation models. These are: smoothness of spiral curvature, spacing of foliation planes, alignment of individual foliation planes within the matrix either side of the porphyroblast and spiral asymmetry with respect to matrix shear sense. Of these four differences, only spiral asymmetry and possibly the alignment of individual foliation planes are diagnostic criteria for distinguishing between the end-member models. None of the four criteria are easily applied in rocks, and testing the mode of spiral origin will only become more reliable with technology that readily enables the 3D reconstruction of spiral geometry. Thus, it is necessary to determine a suite of complementary evidence to distinguish porphyroblast rotation or nonrotation during spiral formation.

ACKNOWLEDGEMENTS

A. Stallard conducted this research with the aid of a JSPS fellowship at Shizuoka University, Japan, and a 'Grant-in-Aid for Scientific Research' from the Japanese Society for the Promotion of Science. The authors acknowledge assistance with MATLAB programming from B. Jagers of Delft Hydraulics, The Netherlands, and M. Robbins of the Canadian Imperial Bank of Commerce. Critical reviews by K. Hickey, N. Gray, S. Johnson and an anonymous reviewer greatly improved the manuscript.

REFERENCES

Bell, T. H., 1985. Deformation partitioning and porphyroblast rotation in metamorphic rocks: a radical reinterpretation. *Journal of Metamorphic Geology*, **3,** 109–118.

Bell, T. H., Forde, A. & Hayward, N., 1992a. Do smoothly curving, spiral-shaped inclusion trails signify porphyroblast rotation? *Geology*, **20,** 59–62.

Bell, T. H., Hickey, K. A. & Upton, G. J. G., 1998. Distinguishing and correlating multiple phases of metamorphism across a multiply deformed region using the axes of spiral, staircase and sigmoidally curved inclusion trails in garnet. *Journal of Metamorphic Geology*, **16,** 767–794.

Bell, T. H. & Johnson, S. E., 1989. Porphyroblast inclusion trails: the key to orogenesis. *Journal of Metamorphic Geology*, **7,** 279–310.

Bell, T. H. & Johnson, S. E., 1992. Shear sense: a new approach that resolves problems between criteria in metamorphic rocks. *Journal of Metamorphic Geology*, **10,** 1–26.

Bell, T. H., Johnson, S. E., Davis, B., Forde, A., Hayward, N. & Wilkins, C., 1992b. Porphyroblast inclusion-trail orientation data: eppure non son girate! *Journal of Metamorphic Geology*, **10,** 295–307.

Biermeier, C., Stuwe, K. & Barr, T., 2001. The rotation rate of cylindrical objects during simple shear. *Journal of Structural Geology*, **23,** 765–776.

Bjornerud, M. G. & Zhang, H., 1994. Rotation of porphyroblasts in non-coaxial deformation: insights from computer simulations. *Journal of Metamorphic Geology*, **12,** 135–139.

Busa, M. D. & Gray, N. H., 1992. Rotated staurolite porphyroblasts in the Littleton Schist at Bolton, Connecticut. *Journal of Metamorphic Geology*, **10,** 627–636.

Forde, A. & Bell, T. H., 1993. The rotation of garnet porphyroblasts around a single fold, Lukmanier Pass, Central Alps: Discussion and reply. *Journal of Structural Geology*, **15,** 1365–1372.

Gray, N. H. & Busa, M. D., 1994. The three-dimensional geometry of simulated porphyroblast inclusion trails: inert-marker, viscous-flow models. *Journal of Metamorphic Geology*, **12,** 575–587.

Hickey, K. A. & Bell, T. H., 1999. Behaviour of rigid objects during deformation and metamorphism: a test using schists from the Bolton syncline, Connecticut, USA. *Journal of Metamorphic Geology*, **17,** 211–228.

Jiang, D., 2001. Reading history of folding from porphyroblasts. *Journal of Structural Geology*, **23,** 1327–1335.

Johnson, S. E., 1990. Lack of porphyroblast rotation in the Otago Schists, New Zealand: implications for crenulation cleavage development, folding and deformation partitioning. *Journal of Metamorphic Geology*, **8,** 13–30.

Johnson, S. E., 1993a. Unravelling the spirals: a serial thin-section study and three-dimensional computer-aided reconstruction of spiral-shaped inclusion trails in garnet porphyroblasts. *Journal of Metamorphic Geology*, **11,** 621–634.

Johnson, S. E., 1993b. Testing models for the development of spiral-shaped inclusion trails in garnet porphyroblasts: to rotate or not to rotate, that is the question. *Journal of Metamorphic Geology*, **11,** 635–659.

Johnson, S. E., 1999. Porphyroblast microstructures: a review of current and future trends. *American Mineralogist*, **84,** 1711–1726.

Johnson, S. E. & Bell, T. H., 1996. How useful are 'millipede' and other similar porphyroblast microstructures for determining synmetamorphic deformation histories? *Journal of Metamorphic Geology*, **14,** 15–28.

Kraus, J. & Williams, P. F., 2001. A new spin on 'non-rotating' porphyroblasts: implications of cleavage refraction and reference frames. *Journal of Structural Geology*, **23,** 963–971.

Mandal, N., Samanta, S. K. & Chakraborty, C., 2001. Numerical modelling of heterogeneous flow fields around rigid objects with special reference to particle paths, strain shadows and foliation drag. *Tectonophysics*, **330,** 177–194.

Mares, V., 1998. Structural development of the Soldiers Cap Group in the Eastern Fold belt of the Mt Isa Inlier: a succession of horizontal and vertical deformation events and large-scale shearing. *Australian Journal of Earth Sciences*, **45,** 373–387.

Masuda, T. & Ando, S., 1988. Viscous flow around a rigid spherical body: a hydrodynamical approach. *Tectonophysics*, **148,** 337–346.

Masuda, T. & Mochizuki, S., 1989. Development of snowmall structure: numerical simulation of inclusion trails during synkinematic porphyroblast growth in metamorphic rocks. *Tectonophysics*, **170,** 141–150.

Passchier, C. W., ten Brink, C. E., Bons, P. & Sokoutis, D., 1993. Delta-objects as a guage for stress sensitivity of strain rate in mylonites. *Earth and Planetary Science Letters*, **120,** 239–245.

Passchier, C. W. & Trouw, R. A. J., 1996. *Microtectonics*. Springer-Verlag, Berlin.

Passchier, C. W., Trouw, R. A. J., Zwart, H. J. & Vissers, R. L. M., 1992. Porphyroblast rotation: eppur si muove? *Journal of Metamorphic Geology*, **10,** 283–294.

Pennacchioni, G., Fasolo, L., Cecci, M. M. & Salasnich, L., 2000. Finite-element modelling of simple shear flow in Newtonian and non-Newtonian fluids around a circular rigid particle. *Journal of Structural Geology*, **22,** 683–692.

Powell, D. & Treagus, J. E., 1967. On the geometry of S-shaped inclusion trails in garnet porphyroblasts. *Mineralogical Magazine*, **36,** 453–456.

Powell, D. & Treagus, J. E., 1970. Rotational fabrics in metamorphic minerals. *Mineralogical Magazine*, **37,** 801–813.
Ramsay, J. G., 1962. The geometry and mechanics of formation of 'similar' type folds. *Journal of Geology*, **70,** 309–327.
Rosenfeld, J. L., 1970. Rotated garnets in metamorphic rocks. *Geological society of America Special Paper*, **129**.
Samanta, S. K., Mandal, N. & Chakraborty, C., 2002. Flow patterns around rigid inclusions in a multiple inclusion system undergoing bulk simple shear deformation. *Journal of Structural Geology*, in press.
Schoneveld, C., 1977. A study of some typical inclusion patterns in strongly paracrystalline-rotated garnets. *Tectonophysics*, **39,** 453–471.
Schoneveld, C., 1978. Syntectonic growth of garnets: discussion of a new model proposed by M.J. de Wit. *Geological Journal*, **13,** 37–46.
Schoneveld, C., 1979. The geometry and significance of inclusion patterns in syntectonic porphyroblasts. *PhD Thesis*, *University of Leiden, The Netherlands*.
Spry, A., 1963. The origin and significance of snowball structures in garnet. *Journal of Petrology*, **4,** 211–222.
Stallard, A. R., 1998. Episodic porphyroblast growth in the Fleur de Lys Supergroup, Newfoundland: timing relative to the sequential development of multiple crenulation cleavages. *Journal of Metamorphic Geology*, **16,** 711–728.
Stallard, A. R. & Hickey, K. H., 2001a. Shear zone vs. folding origin for spiral inclusions in the Canton Schist. *Journal of Structural Geology*, **23,** 1845–1864.
Stallard, A. R. & Hickey, K. H., 2001b. Fold mechanisms in the Canton Schist: constraints on the contribution of flexural flow. *Journal of Structural Geology*, **23,** 1865–1881.
Treagus, J. E., 1987. The structural evolution of the Dalradian of the Central Highlands of Scotland. *Transactions of the Royal Society of Edinburgh*, **78,** 1–15.
Visser, P. & Mancktelow, N. S., 1992. The rotation of garnet porphyroblasts around a single fold, Lukmanier Pass, Central Alps. *Journal of Structural Geology*, **14,** 1193–1202.
Williams, P. F. & Jiang, D., 1999. Rotating garnets. *Journal of Metamorphic Geology*, **17,** 367–378.
Williams, M. L., Scheltema, K. E. & Jercinovic, M. J., 2001. High-resolution compositional mapping of matrix phases: implications for mass transfer during crenulation cleavage development in the Moretown Formation, western Massachusetts. *Journal of Structural Geology*, **23,** 923–939.

Received 22 November 2000; revision accepted 28 May 2002.